EUROPEAN ORGANISATION FOR NUCLEAR RESEARCH

CERN-PPE/95-50
10 April 1995

A Measurement of the Forward-Backward Asymmetry of $e^+e^- \to b\bar{b}$ by Applying a Jet Charge Algorithm to Lifetime Tagged Events

The OPAL Collaboration

Abstract

The forward-backward asymmetry of $e^+e^- \to Z^0 \to b\bar{b}$ has been measured using approximately 2.15 million hadronic Z^0 decays collected at the LEP e^+e^- collider with the OPAL detector. A lifetime tag technique was used to select an enriched $b\bar{b}$ event sample. The measurement of the $b\bar{b}$ asymmetry was then performed using a jet charge algorithm to determine the direction of the primary quark. Values of:

$$\begin{aligned}
A_{\rm FB}^{\rm b} &= 0.062 \pm 0.034 \pm 0.002 - 0.082\,\Delta(\Gamma_{b\bar{b}}/\Gamma_{\rm had}) \quad \text{at } \sqrt{s} = 89.52\,\text{GeV}, \\
A_{\rm FB}^{\rm b} &= 0.0963 \pm 0.0067 \pm 0.0038 - 0.471\,\Delta(\Gamma_{b\bar{b}}/\Gamma_{\rm had}) \quad \text{at } \sqrt{s} = 91.25\,\text{GeV}, \\
A_{\rm FB}^{\rm b} &= 0.172 \pm 0.028 \pm 0.007 - 0.855\,\Delta(\Gamma_{b\bar{b}}/\Gamma_{\rm had}) \quad \text{at } \sqrt{s} = 92.94\,\text{GeV},
\end{aligned}$$

were measured where, in each case, the first error is statistical, the second is systematic and the third term gives the variation due to a change $\Delta(\Gamma_{b\bar{b}}/\Gamma_{\rm had})$ in the value of $\Gamma_{b\bar{b}}/\Gamma_{\rm had} = 0.216$ assumed. The dependence on the assumed charm asymmetry at the same energy is $\Delta(A_{\rm FB}^{\rm b}) \approx +0.07\Delta(A_{\rm FB}^{\rm c})$. Assuming the Standard Model form for the couplings, these measurements correspond to an effective weak mixing angle of:

$$\sin^2\theta_{\rm W}^{\rm eff,e} = 0.2313 \pm 0.0012 \pm 0.0006$$

giving $M_{\rm top} = 196^{+33\,+16}_{-38\,-19}\,\text{GeV}/c^2$, where the first error is statistical and the second is systematic. The Higgs mass assumed is 300 GeV/c^2. A variation in the assumed mass of the Higgs boson between 60 and 1000 GeV/c^2 corresponds to an uncertainty in $\sin^2\theta_{\rm W}^{\rm eff,e}$ of ± 0.00006 and on $M_{\rm top}$ of $^{+20}_{-26}$ GeV/c^2.

(Submitted to Z. Phys. C)

The OPAL Collaboration

R. Akers[16], G. Alexander[23], J. Allison[16], N. Altekamp[5], K. Ametewee[25], K.J. Anderson[9], S. Anderson[12], S. Arcelli[2], S. Asai[24], D. Axen[29], G. Azuelos[18,a], A.H. Ball[17], E. Barberio[26], R.J. Barlow[16], R. Bartoldus[3], J.R. Batley[5], G. Beaudoin[18], S. Bethke[14], A. Beck[23], G.A. Beck[13], C. Beeston[16], T. Behnke[27], K.W. Bell[20], G. Bella[23], S. Bentvelsen[8], P. Berlich[10], J. Bechtluft[14], O. Biebel[14], I.J. Bloodworth[1], P. Bock[11], H.M. Bosch[11], M. Boutemeur[18], S. Braibant[12], P. Bright-Thomas[25], R.M. Brown[20], A. Buijs[8], H.J. Burckhart[8], R. Bürgin[10], C. Burgard[27], P. Capiluppi[2], R.K. Carnegie[6], A.A. Carter[13], J.R. Carter[5], C.Y. Chang[17], C. Charlesworth[6], D.G. Charlton[1,b], S.L. Chu[4], P.E.L. Clarke[15], J.C. Clayton[1], S.G. Clowes[16], I. Cohen[23], J.E. Conboy[15], O.C. Cooke[16], M. Cuffiani[2], S. Dado[22], C. Dallapiccola[17], G.M. Dallavalle[2], C. Darling[31], S. De Jong[12], L.A. del Pozo[8], H. Deng[17], M.S. Dixit[7], E. do Couto e Silva[12], J.E. Duboscq[8], E. Duchovni[26], G. Duckeck[8], I.P. Duerdoth[16], U.C. Dunwoody[8], J.E.G. Edwards[16], P.G. Estabrooks[6], H.G. Evans[9], F. Fabbri[2], B. Fabbro[21], M. Fanti[2], P. Fath[11], F. Fiedler[12], M. Fierro[2], M. Fincke-Keeler[28], H.M. Fischer[3], R. Folman[26], D.G. Fong[17], M. Foucher[17], H. Fukui[24], A. Fürtjes[8], P. Gagnon[6], A. Gaidot[21], J.W. Gary[4], J. Gascon[18], N.I. Geddes[20], C. Geich-Gimbel[3], S.W. Gensler[9], F.X. Gentit[21], T. Geralis[20], G. Giacomelli[2], P. Giacomelli[4], R. Giacomelli[2], V. Gibson[5], W.R. Gibson[13], J.D. Gillies[20], J. Goldberg[22], D.M. Gingrich[30,a], M.J. Goodrick[5], W. Gorn[4], C. Grandi[2], E. Gross[26], G.G. Hanson[12], M. Hansroul[8], M. Hapke[13], C.K. Hargrove[7], P.A. Hart[9], C. Hartmann[3], M. Hauschild[8], C.M. Hawkes[8], R. Hawkings[8], R.J. Hemingway[6], G. Herten[10], R.D. Heuer[8], J.C. Hill[5], S.J. Hillier[8], T. Hilse[10], P.R. Hobson[25], D. Hochman[26], R.J. Homer[1], A.K. Honma[28,a], R. Howard[29], R.E. Hughes-Jones[16], D.E. Hutchcroft[5], P. Igo-Kemenes[11], D.C. Imrie[25], A. Jawahery[17], P.W. Jeffreys[20], H. Jeremie[18], M. Jimack[1], A. Joly[18], M. Jones[6], R.W.L. Jones[8], P. Jovanovic[1], D. Karlen[6], J. Kanzaki[24], K. Kawagoe[24], T. Kawamoto[24], R.K. Keeler[28], R.G. Kellogg[17], B.W. Kennedy[20], B.J. King[8], J. King[13], J. Kirk[29], S. Kluth[5], T. Kobayashi[24], M. Kobel[10], D.S. Koetke[6], T.P. Kokott[3], S. Komamiya[24], R. Kowalewski[8], T. Kress[11], P. Krieger[6], J. von Krogh[11], P. Kyberd[13], G.D. Lafferty[16], H. Lafoux[8], R. Lahmann[17], W.P. Lai[19], D. Lanske[14], J. Lauber[8], J.G. Layter[4], A.M. Lee[31], E. Lefebvre[18], D. Lellouch[26], J. Letts[2], L. Levinson[26], S.L. Lloyd[13], F.K. Loebinger[16], G.D. Long[17], B. Lorazo[18], M.J. Losty[7], X.C. Lou[8], J. Ludwig[10], A. Luig[10], A. Malik[21], M. Mannelli[8], S. Marcellini[2], C. Markus[3], A.J. Martin[13], J.P. Martin[18], T. Mashimo[24], W. Matthews[25], P. Mättig[3], J. McKenna[29], E.A. Mckigney[15], T.J. McMahon[1], A.I. McNab[13], F. Meijers[8], S. Menke[3], F.S. Merritt[9], H. Mes[7], A. Michelini[8], G. Mikenberg[26], D.J. Miller[15], R. Mir[26], W. Mohr[10], A. Montanari[2], T. Mori[24], M. Morii[24], U. Müller[3], B. Nellen[3], B. Nijjhar[16], S.W. O'Neale[1], F.G. Oakham[7], F. Odorici[2], H.O. Ogren[12], N.J. Oldershaw[16], C.J. Oram[28,a], M.J. Oreglia[9], S. Orito[24], F. Palmonari[2], J.P. Pansart[21], G.N. Patrick[20], M.J. Pearce[1], P.D. Phillips[16], J.E. Pilcher[9], J. Pinfold[30], D.E. Plane[8], P. Poffenberger[28], B. Poli[2], A. Posthaus[3], T.W. Pritchard[13], H. Przysiezniak[30], M.W. Redmond[8], D.L. Rees[1], D. Rigby[1], M.G. Rison[5], S.A. Robins[13], N. Rodning[30], J.M. Roney[28], E. Ros[8], A.M. Rossi[2], M. Rosvick[28], P. Routenburg[30], Y. Rozen[8], K. Runge[10], O. Runolfsson[8], D.R. Rust[12], M. Sasaki[24], C. Sbarra[2], A.D. Schaile[8], O. Schaile[10], F. Scharf[3], P. Scharff-Hansen[8], P. Schenk[4], B. Schmitt[3], M. Schröder[8], H.C. Schultz-Coulon[10], P. Schütz[3], M. Schulz[8], J. Schwiening[3], W.G. Scott[20], M. Settles[12], T.G. Shears[16], B.C. Shen[4], C.H. Shepherd-Themistocleous[7], P. Sherwood[15], G.P. Siroli[2], A. Skillman[15], A. Skuja[17], A.M. Smith[8], T.J. Smith[28], G.A. Snow[17], R. Sobie[28], S. Söldner-Rembold[10], R.W. Springer[30], M. Sproston[20], A. Stahl[3], M. Starks[12], C. Stegmann[10], K. Stephens[16], J. Steuerer[28], B. Stockhausen[3], D. Strom[19], P. Szymanski[20], R. Tafirout[18], P. Taras[18], S. Tarem[26], M. Tecchio[9], P. Teixeira-Dias[11], N. Tesch[3], M.A. Thomson[8], E. von Törne[3], S. Towers[6], M. Tscheulin[10], T. Tsukamoto[24], A.S. Turcot[9], M.F. Turner-Watson[8], P. Utzat[11], R. Van Kooten[12], G. Vasseur[21], P. Vikas[18], M. Vincter[28], F. Wäckerle[10], A. Wagner[27], D.L. Wagner[9], C.P. Ward[5], D.R. Ward[5], J.J. Ward[15], P.M. Watkins[1], A.T. Watson[1], N.K. Watson[7], P. Weber[6], P.S. Wells[8], N. Wermes[3], B. Wilkens[10], G.W. Wilson[27], J.A. Wilson[1], T. Wlodek[26], G. Wolf[26], S. Wotton[11], T.R. Wyatt[16], G. Yekutieli[26], V. Zacek[18], W. Zeuner[8], G.T. Zorn[17].

[1]School of Physics and Space Research, University of Birmingham, Birmingham B15 2TT, UK
[2]Dipartimento di Fisica dell' Università di Bologna and INFN, I-40126 Bologna, Italy
[3]Physikalisches Institut, Universität Bonn, D-53115 Bonn, Germany
[4]Department of Physics, University of California, Riverside CA 92521, USA
[5]Cavendish Laboratory, Cambridge CB3 0HE, UK
[6]Carleton University, Department of Physics, Colonel By Drive, Ottawa, Ontario K1S 5B6, Canada
[7]Centre for Research in Particle Physics, Carleton University, Ottawa, Ontario K1S 5B6, Canada
[8]CERN, European Organisation for Particle Physics, CH-1211 Geneva 23, Switzerland
[9]Enrico Fermi Institute and Department of Physics, University of Chicago, Chicago IL 60637, USA
[10]Fakultät für Physik, Albert Ludwigs Universität, D-79104 Freiburg, Germany
[11]Physikalisches Institut, Universität Heidelberg, D-69120 Heidelberg, Germany
[12]Indiana University, Department of Physics, Swain Hall West 117, Bloomington IN 47405, USA
[13]Queen Mary and Westfield College, University of London, London E1 4NS, UK
[14]Technische Hochschule Aachen, III Physikalisches Institut, Sommerfeldstrasse 26-28, D-52056 Aachen, Germany
[15]University College London, London WC1E 6BT, UK
[16]Department of Physics, Schuster Laboratory, The University, Manchester M13 9PL, UK
[17]Department of Physics, University of Maryland, College Park, MD 20742, USA
[18]Laboratoire de Physique Nucléaire, Université de Montréal, Montréal, Quebec H3C 3J7, Canada
[19]University of Oregon, Department of Physics, Eugene OR 97403, USA
[20]Rutherford Appleton Laboratory, Chilton, Didcot, Oxfordshire OX11 0QX, UK
[21]CEA, DAPNIA/SPP, CE-Saclay, F-91191 Gif-sur-Yvette, France
[22]Department of Physics, Technion-Israel Institute of Technology, Haifa 32000, Israel
[23]Department of Physics and Astronomy, Tel Aviv University, Tel Aviv 69978, Israel
[24]International Centre for Elementary Particle Physics and Department of Physics, University of Tokyo, Tokyo 113, and Kobe University, Kobe 657, Japan
[25]Brunel University, Uxbridge, Middlesex UB8 3PH, UK
[26]Particle Physics Department, Weizmann Institute of Science, Rehovot 76100, Israel
[27]Universität Hamburg/DESY, II Institut für Experimental Physik, Notkestrasse 85, D-22607 Hamburg, Germany
[28]University of Victoria, Department of Physics, P O Box 3055, Victoria BC V8W 3P6, Canada
[29]University of British Columbia, Department of Physics, Vancouver BC V6T 1Z1, Canada
[30]University of Alberta, Department of Physics, Edmonton AB T6G 2J1, Canada
[31]Duke University, Dept of Physics, Durham, NC 27708-0305, USA

[a]Also at TRIUMF, Vancouver, Canada V6T 2A3
[b] Royal Society University Research Fellow

1 Introduction

The differential cross-section for the production of fermion-antifermion pairs in e^+e^- annihilation can be expressed as:

$$\frac{d\sigma}{d\cos\theta} \propto 1 + \cos^2\theta + \frac{8}{3} A_{FB} \cos\theta \tag{1}$$

where θ is the angle between the directions of the outgoing fermion and incoming electron, and where mass and higher order terms have been neglected. This form shows explicitly the resulting forward-backward asymmetry, A_{FB}, which is defined by:

$$A_{FB} = \frac{\int_0^{+1} (d\sigma/d\cos\theta)\, d\cos\theta - \int_{-1}^{0} (d\sigma/d\cos\theta)\, d\cos\theta}{\int_{-1}^{+1} (d\sigma/d\cos\theta)\, d\cos\theta}. \tag{2}$$

In the framework of the Standard Model the asymmetry is related directly to v and a, the vector and axial-vector couplings of the electron and fermion, f, to the Z^0 and therefore to the weak mixing angle $\sin^2\theta_W$. At the Z^0 resonance it has the approximate form [1]:

$$A_{FB} \approx \frac{3}{4} \frac{2v_e a_e}{(v_e^2 + a_e^2)} \frac{2v_f a_f}{(v_f^2 + a_f^2)}. \tag{3}$$

The forward-backward asymmetry on the resonance is, neglecting mass effects, the same for all fermions with the same charge. In the Standard Model, the vector and axial-vector couplings may be expressed in terms of the weak mixing parameter, $\sin^2\theta_W^{eff,e}$, where:

$$\frac{v_e}{a_e} = 1 - 4\sin^2\theta_W^{eff,e}, \tag{4}$$

and where v_e/a_e is defined in terms of the electron asymmetry at the Z^0 pole. Hence, measuring A_{FB} allows $\sin^2\theta_W^{eff,e}$ to be determined within the Standard Model. The asymmetry for down-like (d,s,b) quarks has a higher sensitivity to the weak mixing angle than that for up-like (u,c) quarks and charged leptons [1].

The OPAL experiment has already published a measurement of A_{FB}^b based on the identification of prompt leptons originating from heavy flavour decay [2]. Recent results from other LEP experiments are also summarised in [3].

For this measurement, the relatively long lifetime of weakly-decaying hadrons containing a b quark is exploited by seeking secondary vertices, displaced significantly from the interaction point, to obtain an enriched sample of $b\bar{b}$ events. A jet charge method, based on the charge distribution of the final state particles, has been used to distinguish between the direction of the primary quark produced in the decay of the Z^0 and that of the primary antiquark. This method, which will be described in more detail in sections 3 and 4, relies very little on Monte Carlo modelling of the b jet charge since the quantities most relevant for the analysis were measured directly from the data. It makes a statistical determination of the number of forward and backward events. A different analysis, described in section 6, based on a study of the jet charges on an event-by-event basis provided a check of the main analysis. Analyses using the jet charge to determine A_{FB}^b have been reported previously by the ALEPH [4] and DELPHI [5] collaborations.

In general, A_{FB}^b depends on the centre-of-mass energy, $\sqrt{s}$ and this dependence has a well defined functional form in the Standard Model [1]. In this analysis the b-asymmetry was measured for events collected on, and approximately 2 GeV above and below, the Z^0 peak.

2 Event Selection

The analysis described here is based on data recorded with the OPAL detector [6] in the years 1991 to 1994 inclusive. Multihadronic decays of the Z^0 were selected using the criteria described in [7], and were

required to contain at least seven charged tracks passing certain minimum track quality requirements. In addition, the silicon microvertex detector, the central tracking chambers and the electromagnetic calorimeters were required to have been correctly operating when the data were recorded.

For the purposes of b-tagging, charged particle tracks and electromagnetic calorimeter energy clusters not associated to charged tracks were combined into jets using the JADE algorithm [8] with the E0 recombination scheme [9]. An invariant mass-squared cut-off of $x_{\min} = (7\,\mathrm{GeV}/c^2)^2$ was used. According to Monte Carlo simulation, the momentum vectors of the jets found in this manner closely follow the b-hadron direction. The thrust axis was also determined using both tracks and unassociated electromagnetic calorimeter energy clusters and was used as an estimator of the direction of the initial quark-antiquark pair. The analysis was restricted to events largely contained within the silicon microvertex detector acceptance by applying a cut $|\cos\theta_{\mathrm{T}}| < 0.8$ on the polar angle, θ_{T}, of the thrust axis. A sample of approximately 2.15 million events passed these requirements.

The Jetset 7.3 Monte Carlo program [10] was used to generate event samples, which were then processed by a program that simulated the response of the OPAL detector [11]. Smaller samples generated with the HERWIG 5.5 [12] program were also used. Simulated events were processed through the same reconstruction and selection algorithms as were data from the detector. The Lund symmetric fragmentation function [10] was used to describe the hadronisation properties of u, d and s quarks whereas for $\mathrm{b\overline{b}}$ and $\mathrm{c\overline{c}}$ events the fragmentation was described by the function of Peterson *et al.* [13]. The values of the parameters controlling the fragmentation function used for $\mathrm{b\overline{b}}$ and $\mathrm{c\overline{c}}$ events were $\epsilon_{\mathrm{b}} = 0.0055$ and $\epsilon_{\mathrm{c}} = 0.05$, respectively, corresponding to LEP average values of the scaled energies of bottom and charm hadrons of $\langle x_E \rangle_{\mathrm{b}} = 0.70$ and $\langle x_E \rangle_{\mathrm{c}} = 0.51$, respectively [14].

To obtain a highly enriched sample of $\mathrm{b\overline{b}}$ events in the multihadron sample a lifetime tag was used. This was based on the selection of events with secondary vertices that were well separated from the primary vertex. These vertices are expected to be formed mainly by the tracks resulting from b-flavour hadron decays. The primary vertex for each event was reconstructed in the plane transverse to the beam axis using a χ^2 minimization method which also incorporated the average beamspot position as a constraint. The secondary vertex finding algorithm attempts to reconstruct a separate secondary vertex for each jet in the event and is described in [15]. In a first iteration, all charged tracks in a given jet are fitted to a common vertex point in the plane transverse to the beam axis. If one or more tracks contribute $\Delta\chi^2 > 4$ to the overall χ^2 for the secondary vertex fit, then the track with the largest $\Delta\chi^2$ is removed and the fit repeated. The process is continued until all tracks contribute $\Delta\chi^2 < 4$ or until fewer than four tracks remain, in which case the secondary vertex reconstruction fails for this particular jet.

Additional cuts were applied to those charged tracks which were used by the secondary vertex finding algorithm, aimed mainly at removing poorly measured tracks, or tracks from $\mathrm{K^0_S}$ or Λ decays. The point of closest approach of each track to the primary vertex in the plane transverse to the beam axis, d_0, was required to satisfy $|d_0| < 0.3$ cm, while the error on this quantity, $\sigma(d_0)$, was required to satisfy $\sigma(d_0) < 0.1$ cm.

The vertex decay length L was calculated for each reconstructed secondary vertex. L was defined as the distance of the secondary vertex from the primary vertex, constrained by the direction given by the total momentum vector (in the plane transverse to the beam direction) of the jet containing the tracks assigned to the secondary vertex. The total vertex momentum vector was also used to determine the sign of the decay length as follows: $L > 0$ if the secondary vertex was displaced from the primary vertex in the same direction as the total momentum, and $L < 0$ otherwise. Vertices were required to have a reconstructed decay length $|L| < 2$ cm. The quantity L/σ is referred to as the decay length significance, where σ is the error on the determination of the decay length L, which takes into account the uncertainties in the primary and secondary vertex positions. The track parameter resolution was degraded in the Monte Carlo as in [15] to improve the agreement with the data in the region of negative decay length significance, where resolution effects dominate. The effects of changing the degradation factors are included in the systematic uncertainties.

Figure 1 shows the distribution of decay length significance, L/σ, for secondary vertices in the data and Monte Carlo samples. Vertices with large positive values of L/σ are produced dominantly in $b\overline{b}$ events. The Monte Carlo agreement with the data is poor in this region. This difference is ascribed to assumptions in the Monte Carlo about the underlying b quark physics, such as the average b lifetime and decay multiplicity. However, as will be described in detail later, such differences between data and Monte Carlo in this region do not affect the results of the analysis, since the b tagging efficiency is determined directly from data with very little reliance on Monte Carlo modelling.

The hadronic events were divided into two hemispheres by the plane perpendicular to the thrust axis and containing the interaction point. The *forward thrust hemisphere* is defined to be the one that contains the positive z axis[1] and the other hemisphere is called the *backward thrust hemisphere*. To ensure a good charge reconstruction, only events having more than three good charged tracks per hemisphere were used. Each hemisphere was deemed to give a lifetime tag if it contained at least one reconstructed secondary vertex which satisfied the requirements described above and had a decay length significance $L/\sigma > 8$. In total 165 771 events passed the lifetime tag. Within these events, 180 499 tagged hemispheres were found and there were 14 728 events in which both hemispheres were tagged. The $e^+e^- \rightarrow b\overline{b}$ events made up 90.2% of the tagged event sample.

The peak events were defined as those with $\sqrt{s}$ between 91.05 and 91.40 GeV. Those below the peak had energies between 88.4 and 90.4 GeV and those above the peak had energies ranging from 92.0 to 94.0 GeV. The corresponding luminosity-weighted mean centre-of-mass energies of the three classes were, 89.52, 91.25 and 92.94 GeV, respectively.

3 The Jet Charge Method

To measure the forward-backward asymmetry it is necessary to determine the number of forward and backward events in the sample. In the jet charge method the thrust axis was used to divide events into a forward thrust hemisphere and a backward thrust hemisphere (as discussed in the previous section) and a momentum weighted charge sum calculated in each. These charge sums reflect the charge of the primary parton contained in the hemisphere. The difference between the charge sums in the forward and backward thrust hemispheres was then calculated, and the number of forward and of backward events in the sample are obtained by comparing the mean value of this difference with those expected for forward and for backward event samples.

For each hemisphere, defined by the direction of the thrust axis, the jet charge, Q_{jet} [16] is computed as:

$$Q_{jet} = \frac{\sum_i^N |p_{||_i}|^\kappa q_i}{\sum_i^N |p_{||i}|^\kappa} \tag{5}$$

where the sum runs over the N charged tracks of the hemisphere, $p_{||_i}$ is the momentum component of the track i along the thrust axis, q_i is the charge of track i and κ is a parameter which controls the momentum weighting of each particle's charge. The weighting used here in order to optimise the charge determination is $\kappa = 0.5$. Only tracks with transverse momentum with respect to the beam direction greater than 0.15 GeV/c were used to compute the jet charge. The jet charges in the forward and backward thrust hemispheres, defined in section 2, are labelled Q_F and Q_B respectively.

This analysis makes use of the mean jet charge separation between forward and backward hemispheres to measure the forward-backward asymmetry. For a given sample of events the *mean charge separation* is defined as:

$$\delta = \langle Q_- - Q_+ \rangle \tag{6}$$

where Q_- and Q_+ are the jet charges measured in the thrust hemispheres with the negatively charged quark and positively charged quark respectively, and the average is over all events in the sample.

[1] The OPAL coordinate system is defined with positive z along the electron beam direction with θ and ϕ being the polar and azimuthal angles, respectively. The origin is in the centre of the detector, which is the nominal interaction point.

From the data one can measure the quantity $\langle Q_F - Q_B \rangle$. For a sample consisting of a single type i of down-like quark, where there are N_F events with the negative quark in the forward thrust hemisphere and N_B events with the negative quark in the backward thrust hemisphere, then:

$$\begin{aligned} \langle Q_F - Q_B \rangle_i &= \frac{N_F \langle Q_- - Q_+ \rangle_i + N_B \langle Q_+ - Q_- \rangle_i}{N_F + N_B} \\ &= \frac{N_F - N_B}{N_F + N_B} \cdot \langle Q_- - Q_+ \rangle_i \\ &= A_i \cdot \delta_i \end{aligned} \tag{7}$$

where the suffix i denotes the quark flavour, A_i is the forward-backward charge asymmetry in the sample and δ_i is the mean charge separation.

For a sample consisting of a mixture of flavours, as in the lifetime tagged sample, the value of $\langle Q_F - Q_B \rangle$ of the whole sample can be related to the individual asymmetries and charge separations using the relationship:

$$\begin{aligned} \langle Q_F - Q_B \rangle &= \sum_i s_i F_i \delta_i A_i \\ &= \sum_i s_i F_i \delta_i C_i A^i_{\mathrm{FB}} \end{aligned} \tag{8}$$

where the suffix i denotes the quark flavour and the sum is over all flavours. The value of s_i is defined as $+1$ for the down-like quarks and -1 for the up-like quarks. The fractions of each quark flavour in the sample are denoted by F_i. The factors C_i correct from the total forward-backward asymmetry for events of a given flavour, A^i_{FB}, to that of those in the sample, A_i, a correction which is dominated by the finite angular acceptance. These factors C_i are described in more detail in section 3.1.

The charge separation, δ, can be measured almost entirely from the data sample. For the case of no bias in the charge identification between positive and negative primary quarks, and assuming no correlation between Q_- and Q_+, it follows that:

$$\left(\frac{\delta}{2}\right)^2 = \langle Q_- \rangle \cdot \langle -Q_+ \rangle = -\langle Q_- \cdot Q_+ \rangle = -\langle Q_F \cdot Q_B \rangle.$$

Taking into account the effects of possible charge bias and correlations between Q_- and Q_+, one obtains (see Appendix A.):

$$\delta^2 = 4 \frac{-\langle Q_F \cdot Q_B \rangle + \rho[Q_-, Q_+]\sigma^2(Q) + \mu^2(Q)}{1 + \rho[Q_-, Q_+]} \tag{9}$$

where $\mu(Q)$ and $\sigma^2(Q)$ are the mean and variance of the charge of all hemispheres and $\rho[Q_-, Q_+]$ is the charge correlation between Q_- and Q_+. This correlation is due to overall charge conservation in the event, and to migration of particles between the quark and the antiquark hemisphere. Only the correlation coefficient $\rho[Q_-, Q_+]$ has to be estimated from Monte Carlo since all other quantities can be taken directly from data. Equation 9 takes into account small differences between the jet charge for positive and negative quarks introduced by the detector (*via* the $\mu^2(Q)$ term) but does assume that $\sigma(Q_-) = \sigma(Q_+)$. This assumption has been checked using Monte Carlo and found to be a very good approximation.

Equation 9 can be applied to a mixed sample of events or to a sample consisting of just one flavour. In the case of the lifetime tagged events, the charge separation of the sample, δ^{tagged}, can be related to the individual charge separations for each quark flavour, i, *via*:

$$\delta^{\mathrm{tagged}} = \sum_i F_i \delta_i. \tag{10}$$

Hence, from $\delta^{\rm tagged}$ it is possible to extract δ_b. The fraction of each flavour in the tagged sample and the charge separation and asymmetry for charm and light quarks must be taken from elsewhere. It should be emphasised that the lifetime tagged sample is comprised of approximately 90% $\rm b\overline{b}$ events and therefore only small systematic errors are introduced by the assumptions that are made about the non-b component of the sample. Since δ_b already includes the effect of $\rm B^0\overline{B^0}$ mixing and biases due to lifetime tagging the asymmetry measurement is insensitive to these effects. This value of δ_b can then be used in Equation 8 to calculate the $\rm b\overline{b}$ forward-backward asymmetry.

As a mean quantity is used to measure the asymmetry, it is in effect a counting method, as is apparent from Equation 7. However, in the case of the measurement of the asymmetry at the $\rm Z^0$ peak, the high statistics available allow a gain in precision by performing the measurement separately in several regions of $|\cos\theta_{\rm T}|$. The additional information from the variation of the $\langle Q_F - Q_B \rangle$ with angle adds precision to the overall asymmetry measurement.

3.1 Correction Factors

The forward-backward asymmetry as defined in Equation 1 is that of a sample with an unlimited acceptance, and is predicted in terms of the direction of the outgoing primary quark. This analysis used a sample of events selected within a finite geometrical acceptance, and used the direction of the experimentally determined thrust axis to estimate the direction of the primary quark and to define the event hemispheres. In addition, the selection and tagging efficiency for each flavour of event was not uniform within the acceptance, and differed between the flavours. There was also a reduction in the observed charge separation for events near to the edge of the acceptance, due to tracks failing the cuts. All of these experimental effects were corrected for using the factors C_i introduced in Equation 8, which relate the forward-backward asymmetry for a given flavour i, $A^i_{\rm FB}$, to that measured in the tagged sample, A_i. The dominant correction is for the geometrical acceptance.

Detector resolutions and efficiencies mean that the calculated polar angle of the thrust axis, $\theta_{\rm T}$, is a smeared estimator both of the polar angle of the true thrust axis of all final state particles, $\theta_{\rm T}^{\rm true}$, and of the polar angle of the outgoing primary quark, $\theta_{\rm T}^{\rm quark}$. It is also biased towards smaller values of $|\cos\theta_{\rm T}|$ for large $|\cos\theta_{\rm T}^{\rm true}|$ or $|\cos\theta_{\rm quark}|$. Hence, the differential cross-section in $\cos\theta_{\rm T}$ does not follow the form of Equation 1, while the Monte Carlo samples indicate that the differential cross sections in $\cos\theta_{\rm T}^{\rm true}$ and in $\cos\theta_{\rm quark}$ do have this form. In the following sections, asymmetries $A^{\rm b}_{\rm FB}$ defined in terms of $\cos\theta_{\rm T}^{\rm true}$ are presented. These measured asymmetries had experimental effects removed in a way that was largely insensitive to the Monte Carlo model used. However, the Standard Model predictions are of the asymmetry defined in terms of $\cos\theta_{\rm quark}$, and it is this which is needed to extract $\sin^2\theta_{\rm W}^{\rm eff,e}$. In addition to correcting for detector resolutions and efficiencies, and acceptance and selection requirements, obtaining the asymmetry in terms of $\cos\theta_{\rm quark}$ entails corrections for the effects of decay and fragmentation, and for QCD radiative effects, which are somewhat model-dependent.

It should be noted that the fact that the hemisphere definition used in determining $\langle Q_F - Q_B \rangle$ is based on the experimentally measured thrust axis inherently corrects for some of the QCD radiative effects. This is because when hard gluon radiation forces both the b and the $\overline{\rm b}$ into the same event hemisphere, the result is a near-zero measured charge in both hemispheres. The charge separation in these events is therefore small and they contribute little to the measured $\langle Q_F - Q_B \rangle$ and δ and hence to the measured asymmetry. The extent of the residual QCD corrections not already accounted for by this charge-dilution effect must be estimated with the Monte Carlo models.

The factors C_i used to correct from the experimental to the true thrust direction, and for the $\cos\theta_{\rm T}$ cut, were calculated assuming the differential cross-section form of Equation 1:

$$C_i = \frac{8}{3}\frac{\int_0^1 a_i(y)\delta_i(y)y{\rm d}y}{\int_0^1 a_i(y)\delta_i(y)(1+y^2){\rm d}y} \tag{11}$$

where $y = |\cos\theta_{\rm T}^{\rm true}|$, $a_i(y)$ is a combined event acceptance, selection and lifetime tagging efficiency function for flavour i, and δ_i is the charge separation of events of flavour i passing the acceptance,

selection and tagging requirements. The tagging efficiency as a function of $|\cos\theta_{\rm T}|$ for b-events was measured from the data in bins of $|\cos\theta_{\rm T}|$ and reweighted to give the tagging efficiency as a function of $|\cos\theta_{\rm T}^{\rm true}|$ using Monte Carlo information. The tagging efficiency shape determined from the data for b-events was also assumed for the charm events, as they are very similar in the Monte Carlo. The direct determination of the charm efficiency function from the data has large statistical errors but is consistant with this assumption. For the light quarks the Monte Carlo was used to estimate the efficiency as a function of $|\cos\theta_{\rm T}^{\rm true}|$ directly. The effect of the acceptance and selection requirements (before the tagging algorithm was applied) was taken from the Monte Carlo for all quark flavours and then combined with the tagging efficiencies to obtain the functions $a_i(y)$. The factors C_i are only slightly sensitive to the shape of the distributions $\delta_i(y)$, which were taken from the Monte Carlo, and were independent of their normalisation. Example values for the factors C_i for the on-peak data are given in Table 1. The values obtained were very similar to those calculated assuming a uniform tagging and selection efficiency for all quarks, no charge dilution and perfect estimation of the quark direction, *i.e.* those just correcting for the limited geometrical acceptance, $C^{\rm geom}$, which are given for the relevant $|\cos\theta|$ ranges in Table 2.

	C_i	$C_i^{\rm quark}$
b	0.855 ± 0.003	0.846 ± 0.003
c	0.855 ± 0.010	0.846 ± 0.010
u, d, s	0.897 ± 0.008	0.878 ± 0.008

Table 1: The on-peak event-weighted average asymmetry correction factors appropriate for the thrust axis asymmetry (C_i) and the quark direction asymmetry ($C_i^{\rm quark}$) when measured for events with a $|\cos\theta_{\rm T}| < 0.8$. The errors quoted for u, d and s are purely statistical.

	$\lvert\cos\theta\rvert$ range				
	0.0–0.2	0.2–0.4	0.4–0.6	0.6–0.8	0.0–0.8
$C^{\rm geom}$	0.2632	0.7317	1.0638	1.2500	0.8791

Table 2: The correction factors, $C^{\rm geom}$, correcting for a limited geometrical acceptance, assuming a uniform efficiency as a function of polar angle and perfect reconstruction of the outgoing fermion direction. These factors are not used in the analysis, and are shown only for illustrative purposes.

The correction factors used to obtain the asymmetry defined in terms of $\cos\theta_{\rm quark}$, $C_i^{\rm quark}$, were obtained in a similar way to the C_i. However, because of the difference between $|\cos\theta_{\rm quark}|$ and $|\cos\theta_{\rm T}|$, a forward-going quark ($\cos\theta_{\rm quark} > 0$) can be assigned to the backward thrust hemisphere, and *vice versa*, particularly for $|\cos\theta_{\rm quark}| \approx 0$; this effect will be referred to as 'flipping'. The flipped events have an opposite asymmetry and a different mean charge separation δ to the unflipped events, and so the two event classes are treated separately when calculating the $C_i^{\rm quark}$. The correction factors to give the quark asymmetry are sensitive to the precise nature of the gluon radiation assumed in the generator models. Examples of the correction factors $C_i^{\rm quark}$ obtained are given in Table 1. They are very similar to those evaluated when correcting to obtain the asymmetry calculated in terms of the true thrust axis, and hence also to the $C_i^{\rm geom}$ values given in Table 2.

4 Analysis and Results

4.1 The Composition of the Tagged Sample

The composition of the tagged sample must be known so that a correction can be made for the small contamination of non-b events. To extract the fractions of each flavour, F_i, a double tag technique similar to that described in [15] was used. The number of tagged hemispheres, N_t, and the number of events in which both hemispheres are tagged, N_{2t}, can be expressed as:

$$N_t = 2N_{\rm had}\left(\frac{\Gamma_{\rm b\overline{b}}}{\Gamma_{\rm had}}\eta_{\rm b} + \frac{\Gamma_{\rm c\overline{c}}}{\Gamma_{\rm had}}\eta_{\rm c} + \frac{\Gamma_{\rm u\overline{u}}}{\Gamma_{\rm had}}\eta_{\rm u} + \frac{\Gamma_{\rm d\overline{d}}}{\Gamma_{\rm had}}\eta_{\rm d} + \frac{\Gamma_{\rm s\overline{s}}}{\Gamma_{\rm had}}\eta_{\rm s}\right) \tag{12}$$

$$N_{2t} = N_{\rm had}\left(\frac{\Gamma_{\rm b\overline{b}}}{\Gamma_{\rm had}}\eta_{\rm b}^2\rho_{\rm b} + \frac{\Gamma_{\rm c\overline{c}}}{\Gamma_{\rm had}}\eta_{\rm c}^2\rho_{\rm c} + \frac{\Gamma_{\rm u\overline{u}}}{\Gamma_{\rm had}}\eta_{\rm u}^2\rho_{\rm u} + \frac{\Gamma_{\rm d\overline{d}}}{\Gamma_{\rm had}}\eta_{\rm d}^2\rho_{\rm d} + \frac{\Gamma_{\rm s\overline{s}}}{\Gamma_{\rm had}}\eta_{\rm s}^2\rho_{\rm s}\right) \tag{13}$$

where $N_{\rm had}$ is the number of multihadronic events and η_i are the hemisphere tagging efficiencies for the different flavours. The ρ_i are correlation factors which describe the correlation between the probabilities of tagging each of the hemispheres in a given event. The correlation factors for each flavour i can be expressed in terms of the single hemisphere tagging efficiency η_i and the efficiency of double tagging an event, η_i^{dt}, as:

$$\rho_i = \frac{\eta_i^{dt}}{\eta_i^2} \tag{14}$$

For the cuts applied, the correlation factors are close to unity. As the b-fraction of the sample is approximately 90%, even large deviations from unity of $\rho_{\rm u}$, $\rho_{\rm d}$, $\rho_{\rm s}$ and $\rho_{\rm c}$ do not affect the measurement of $A_{\rm FB}^{\rm b}$. Hence, for the central value, only the effect of hemisphere correlations for b quark events were included. For small deviations from unity, the correlation factor can be expressed as $\rho_{\rm b} = 1 + \Delta\rho_{\rm b}{}^{\rm geom} + \Delta\rho_{\rm b}{}^{\rm phys}$, where $\Delta\rho_{\rm b}{}^{\rm geom}$ comes purely from the geometry of the detector and $\Delta\rho_{\rm b}{}^{\rm phys}$ comes from the underlying physics processes. The correlation $\Delta\rho_{\rm b}{}^{\rm geom}$ due to non-uniform tagging efficiency as a function of $\cos\theta_{\rm T}$ and ϕ was calculated from the data. This was done separately for the data taken with the two different versions of the silicon microvertex detector and for each year's data, for which the overall efficiency was different. The two bottom hadrons in a $\rm b\overline{b}$ event are likely to be produced back-to-back and their decay products are therefore likely to strike geometrically opposite parts of the detector. This introduces a correlation if the efficiency of the detector is not completely uniform. This correlation was estimated by measuring the hemisphere tagging probability for the real data in small bins of $|\cos\theta|$ and ϕ of the thrust axis direction:

$$\Delta\rho_{\rm b}{}^{\rm geom} = \frac{\sum_\theta\sum_\phi(N(\theta,\phi)f_F(\theta,\phi)f_B(\theta,\phi))/N}{\left(\sum_\theta\sum_\phi(N(\theta,\phi)(f_F(\theta,\phi)+f_B(\theta,\phi)))/2N\right)^2} - 1 \tag{15}$$

where N is the total number of events, $N(\theta,\phi)$ is the number of events in each bin and $f_F(\theta,\phi)$ and $f_B(\theta,\phi)$ are the fraction of tagged hemispheres in the forward and backward hemispheres respectively. The correlation $\Delta\rho_{\rm b}{}^{\rm geom}$ was estimated to be 0.0131 ± 0.0012 for the data taken in 1991 and 1992, 0.0268 ± 0.0019 for the data taken in 1993, and 0.0215 ± 0.0011 for that taken in 1994. The errors are statistical. The values differ due to known changes in the efficiency of the OPAL tracking system.

Other sources of correlation, represented by the term $\Delta\rho_{\rm b}{}^{\rm phys}$, were investigated using Monte Carlo simulations. Those considered were the momentum-momentum correlation between the b-hadrons produced from the b and $\overline{\rm b}$ quarks, and the negative correlations due to hard gluon radiation (which tends to reduce the back-to-back nature of the event). The correlation factor $\Delta\rho_{\rm b}{}^{\rm phys}$ due to these effects is $\Delta\rho_{\rm b}{}^{\rm phys} = -0.0008 \pm 0.0060$. The overall correlation factor is $\rho_{\rm b} = 1.0123 \pm 0.0061$ for the 1991 and 1992 data, 1.0260 ± 0.0062 for the 1993 data, and 1.0207 ± 0.0061 for the 1994 data.

The analysis procedure was:

- N_t, N_{2t} and $N_{\rm had}$ were measured from data
- $\rho_{\rm b}$ was estimated from data and Monte Carlo
- $\eta_{\rm u}$, $\eta_{\rm d}$ and $\eta_{\rm s}$ were estimated from Monte Carlo simulation
- the hadronic partial widths were taken from the Standard Model prediction; there is a small flavour bias in the event selection, which is taken from the Monte Carlo predictions
- Equations 12 and 13 were solved for $\eta_{\rm b}$ and $\eta_{\rm c}$
- the hemisphere tagging efficiencies η_i were converted into the event tagging efficiencies $\overline{\eta_i}$ using the relation $\overline{\eta_i} = 2\eta_i(1 - \eta_i \cdot \rho_i) + \rho_i \cdot \eta_i^2$
- the fraction of flavour i present in the sample, F_i, was extracted using the relation:

$$F_i = \frac{\overline{\eta_i}\,\Gamma_i/\Gamma_{\rm had}}{\sum_k \overline{\eta_k}\Gamma_k/\Gamma_{\rm had}} \tag{16}$$

  where k runs over all the five flavours.

Table 3 summarises the tagging efficiencies and the corresponding fractions for the various flavours present in the sample of tagged events.

Event Type	Tagging Efficiency $\overline{\eta_i}$	Fraction F_i
$\rm b\overline{b}$	0.3192 ± 0.0013	0.9015 ± 0.0036
$\rm c\overline{c}$	0.0267 ± 0.0016	0.0601 ± 0.0036
$\rm u\overline{u}$	0.0047 ± 0.0001	0.0105 ± 0.0003
$\rm d\overline{d}$	0.0047 ± 0.0001	0.0134 ± 0.0004
$\rm s\overline{s}$	0.0050 ± 0.0001	0.0145 ± 0.0004

Table 3: Event tagging efficiencies and fractions in the data sample (all beam energies are included). The errors are from Monte Carlo statistics for u,d and s. For $\rm b\overline{b}$ and $\rm c\overline{c}$ events the tagging efficiencies were estimated from the data and the errors include only data and Monte Carlo statistical effects.

4.2 Assumed Standard Model Values

The small level of contamination from non-b events in the tagged sample must be corrected for, and requires a knowledge of their partial hadronic widths in $\rm Z^0$ decay and their asymmetries. Some of this information is constrained by experimental data, but in other cases the Standard Model must be assumed. When fitting for $\sin^2\theta_{\rm W}^{\rm eff,e}$ in the context of the Standard Model, these parameters are known exactly, and so introduce no systematic uncertainty.

For the central values, the Standard Model predictions for the partial hadronic widths of the $\rm Z^0$ into $\rm u\overline{u}$, $\rm d\overline{d}$, $\rm s\overline{s}$, $\rm c\overline{c}$ and $\rm b\overline{b}$, and for the asymmetries in non-b events are used. These were obtained using the program ZFITTER (version 4.8) [17], with $M_{\rm Z} = 91.187$ GeV/c^2, $M_{\rm top} = 169$ GeV/c^2, $M_{\rm Higgs} = 300$ GeV/c^2, and $\alpha_s = 0.12$ [18]. These predicted values were then varied and the gradient of the measured asymmetries with respect to each of the assumed parameters determined. Given that the variations of the measured asymmetries are essentially linear in each of the assumed Standard Model parameters, it is then possible to calculate the asymmetries that would be obtained for different sets of assumed Standard Model parameters. Table 4 summarises the central values of the Standard Model parameters which were used.

Event Type	$\Gamma_i/\Gamma_{\rm had}$	$A_{\rm FB}(\sqrt{s}$=89.52 GeV)	$A_{\rm FB}(\sqrt{s}$=91.25 GeV)	$A_{\rm FB}(\sqrt{s}$=92.94 GeV)
$b\bar{b}$	0.216	–	–	–
$c\bar{c}$	0.173	−0.0316	0.061	0.120
$u\bar{u}$	0.173	−0.0315	0.061	0.120
$d\bar{d}$	0.220	0.057	0.093	0.116
$s\bar{s}$	0.220	0.057	0.093	0.116

Table 4: Standard Model parameters used in the analysis. All values are as predicted by ZFITTER version 4.8 using input parameters as determined in [18].

4.3 Results

Event Type	Charge Separation δ_i
$b\bar{b}$	-0.132 ± 0.001
$c\bar{c}$	-0.141 ± 0.004
$u\bar{u}$	-0.212 ± 0.009
$d\bar{d}$	-0.110 ± 0.008
$s\bar{s}$	-0.137 ± 0.007

Table 5: Charge separations for the various flavours. The values quoted for $b\bar{b}$ were determined from the data, whereas for the other flavours they were obtained from Monte Carlo. The errors are statistical only.

Monte Carlo studies indicate that the δ and $\langle Q_F \cdot Q_B \rangle$ are independent of $\sqrt{s}$ over the small range of the data. Thus, they are measured from combined on- and off-peak data. The mean forward-backward charge product was found to be $\langle Q_F \cdot Q_B \rangle = -0.00569 \pm 0.00010$, and $\mu(Q) = 0.00526 \pm 0.00035$, while $\sigma^2(Q) = 0.0418 \pm 0.0004$, where the errors are statistical only. The mean charge separation for the tagged sample was obtained using equation 9 and the Monte Carlo prediction that $\rho[Q_-, Q_+] = -0.035$, and found to be:

$$\delta^{\rm tagged} = -0.1332 \pm 0.0013 \qquad (17)$$

where again the error is statistical only. The negative solution to the equation is taken to correspond to Monte Carlo prediction and naive expectations. It has been confirmed by using leptons from b-decays in one hemisphere to infer the sign of the charge of the parton in the opposite hemisphere; the mean jet charge in the opposite hemisphere is found to have the same sign as the expected parton charge, implying that δ indeed should have a negative sign. This value is then corrected using the known fractions of the different quark flavours, and the δ values for the non-b events (obtained from Jetset and given in Table 5) to obtain the value of $\delta_{\rm b}$ for the sample (also given in Table 5).

For the three different centre-of-mass energy samples, the following charge separations were obtained:

$$\begin{aligned}
\langle Q_F - Q_B \rangle &= -0.0069 \pm 0.0038 \quad \text{at } \sqrt{s} = 89.52\,\text{GeV}, \\
\langle Q_F - Q_B \rangle &= -0.0092 \pm 0.0008 \quad \text{at } \sqrt{s} = 91.25\,\text{GeV}, \\
\langle Q_F - Q_B \rangle &= -0.0172 \pm 0.0032 \quad \text{at } \sqrt{s} = 92.94\,\text{GeV}.
\end{aligned}$$

By applying Equations 8 and 10, the asymmetries based on the true thrust axis, were determined:

$$\begin{aligned}
A_{\rm FB}^{\rm b} &= 0.062 \pm 0.034 \quad \text{at } \sqrt{s} = 89.52\,\text{GeV}, \\
A_{\rm FB}^{\rm b} &= 0.0935 \pm 0.0074 \quad \text{at } \sqrt{s} = 91.25\,\text{GeV}, \\
A_{\rm FB}^{\rm b} &= 0.172 \pm 0.028 \quad \text{at } \sqrt{s} = 92.94\,\text{GeV},
\end{aligned}$$

where the errors are statistical only. The statistical error includes the statistical uncertainties on the fractions of the different flavours, F_i. The prescription for calculating the statistical error is taken from [19], with a small ($\sim 2\%$) correction to take into account the correlation between $\langle Q_F - Q_B \rangle$ and δ.

$\lvert\cos\theta_{\rm T}\rvert$ range	$\langle Q_F - Q_B \rangle$	$\delta^{\rm tagged}$
0.0–0.2	-0.0022 ± 0.0016	-0.133 ± 0.003
0.2–0.4	-0.0073 ± 0.0016	-0.126 ± 0.003
0.4–0.6	-0.0115 ± 0.0015	-0.136 ± 0.003
0.6–0.8	-0.0153 ± 0.0016	-0.137 ± 0.003
0.0–0.8	-0.0092 ± 0.0008	-0.1332 ± 0.0013

Table 6: The on-peak $\langle Q_F - Q_B \rangle$ and charge separation, $\delta^{\rm tagged}$, for the tagged sample in each $\lvert\cos\theta_{\rm T}\rvert$ bin.

Additional precision for the peak asymmetry has been obtained by repeating the analysis in four bins of $\lvert\cos\theta_{\rm T}\rvert$ and forming the weighted average of the results. The extra information is provided by the variation of the measured $\langle Q_F - Q_B \rangle$ with $\lvert\cos\theta_{\rm T}\rvert$. The different values of $\langle Q_F - Q_B \rangle$ and the δ of the tagged sample in each $\lvert\cos\theta_{\rm T}\rvert$ bin are given in Table 6. The resulting asymmetries (which are each corrected to the full acceptance) are presented in Fig. 2, where the errors shown are purely statistical. The result in each bin is statistically compatible with that using all events. The weighted average gives:

$$A_{\rm FB}^{\rm b} = \quad 0.0963 \pm 0.0067 \quad \text{at } \sqrt{s} = 91.25\,\text{GeV},$$

where the error is statistical only.

The measured asymmetries corrected to the thrust axis of all final state particles are thus:

$$\begin{aligned} A_{\rm FB}^{\rm b} &= \quad 0.062 \quad \pm \quad 0.034 \quad \text{at } \sqrt{s} = 89.52\,\text{GeV}, \\ A_{\rm FB}^{\rm b} &= \quad 0.0963 \quad \pm \quad 0.0067 \quad \text{at } \sqrt{s} = 91.25\,\text{GeV}, \\ A_{\rm FB}^{\rm b} &= \quad 0.172 \quad \pm \quad 0.028 \quad \text{at } \sqrt{s} = 92.94\,\text{GeV}, \end{aligned}$$

where the errors are statistical only. The correction to unfold the quark asymmetry from the asymmetry obtained using the thrust axis is provided by the factors $C_i^{\rm quark}$ described in Section 3.1 and given in Table 1. Thus, the Jetset 7.3 Monte Carlo is used to describe the detector smearing, the hadronisation effects and the effects of final-state photon and of gluon radiation. This full correction leads to a larger asymmetry than that when correcting to the true thrust axis of all final state particles. The corresponding b quark asymmetries determined using the quark axis were 0.063, 0.0973 and 0.173, respectively, with the same statistical errors as for the true thrust axis results.

5 Systematic Errors

The systematic errors on $A_{\rm FB}^{\rm b}$ are summarised in Table 7. They are discussed in more detail in the following sections.

5.1 Jet Charge Identification

The uncertainties due to modelling of fragmentation on the u, d, s and c jet charge properties were estimated using Monte Carlo events generated with different fragmentation parameters. The parameter variations [10] are given in Table 8. Most are similar to those in our previous publication on the forward-backward charge asymmetry of hadronic Z^0 decays [20]. In addition to these, the Jetset

	$\sqrt{s}$ = 89.52 GeV	$\sqrt{s}$ = 91.25 GeV	$\sqrt{s}$ = 92.94 GeV
fragmentation modelling	± 0.0011	± 0.0024	± 0.0044
b decay multiplicity	± 0.0003	± 0.0005	± 0.0006
Jet Charge identification	± 0.0011	± 0.0025	± 0.0044
acceptance model	± 0.0005	± 0.0008	± 0.0014
material asymmetry	± 0.0005	± 0.0007	± 0.0014
u, d and s efficiency	± 0.0003	± 0.0004	± 0.0012
efficiency $\cos\theta_{\rm T}$ dependence	± 0.0003	± 0.0004	± 0.0008
hemisphere correlation	± 0.0001	± 0.0005	± 0.0011
r-ϕ detector resolution	± 0.0010	± 0.0014	± 0.0023
$\cot\theta$ detector resolution	± 0.0010	± 0.0015	± 0.0028
thrust direction resolution	$+0.0007$	$+0.0010$	$+0.0018$
Detector effects	± 0.0018	± 0.0026	± 0.0049
Monte Carlo Statistics	± 0.0003	± 0.0013	± 0.0024
Total systematic error	± 0.0021	± 0.0038	± 0.0070
Statistical error	± 0.0337	± 0.0067	± 0.0282

Table 7: Uncertainties on the determination of $A_{\rm FB}^{\rm b}$ below, on and above the peak. Where appropriate, the boldface items represent the sum of the items in the previous section.

baryon direct production parameter and the parameter controlling the rate of baryon production by the 'popcorn' mechanism were also varied. The effect of turning off $\rm B^0\overline{B^0}$ mixing was also considered. The standard mixing parameters for the Monte Carlo generations were $x_{\rm d} = 0.7$ and $x_{\rm s} = \infty$, where $x_{\rm d} = |m_1 - m_2|/\tau(\rm B_d^0)$, m_1 and m_2 are the masses of the two mass eigenstates of the $\rm B_d^0$ and $\tau(\rm B_d^0)$ its lifetime; $x_{\rm s}$ is the corresponding parameter for the mixing in the $\rm B_s^0$ system.

The fragmentation model influences the result in two ways: through the non-b quark δ values; and through the charge correlation coefficient, $\rho[Q_-, Q_+]$. The overall relative uncertainty on the δ values is about 10%, with the ϵ_c, popcorn and $[V/(V+S)]_{\rm u,d}$ (the parameter controlling the rate of vector meson production in u and d fragmentation) contributions largest, while the relative uncertainty on the correlation is about 8%, with the mixing and $[V/(V+S)]_{u,d}$ contributions largest. The systematic uncertainties from each of the parameter variations in Table 8 are combined in quadrature.

The effects of incorrect modelling of the b-decay multiplicities were investigated. The b-decay multiplicity per thrust hemisphere was varied by the OPAL measured uncertainty of 0.51 [21], which corresponds to approximately 10%, to which an additional multiplicity variation of 0.25 has been added to account for the observed multiplicity bias in tagged hemispheres. The effects on the final result are small. This is because the correlation coefficient, $\rho[Q_-, Q_+]$, is insensitive to such modelling effects.

The effect of varying the charm decay multiplicity by ± 0.14, a range suggested in [21], is negligible.

5.2 Detector Effects

The acceptances for $\rm Z^0$ decays to the different quark flavours are predicted to differ by small amounts in the Monte Carlo simulations. The central value for the asymmetry is obtained using the predictions of Jetset 7.3. The resulting change in the measured $A_{\rm FB}^{\rm b}$ when the predictions of HERWIG 5.5 are used are taken as an estimate of the systematic uncertainty in these acceptances.

The analysis assumes that within the experimental acceptance the material in front of the tracking detectors is symmetric in $\cos\theta_{\rm T}$, which is true within the statistical precision in the Monte Carlo samples. Any material asymmetry can lead to an apparent forward-backward charge asymmetry in

Parameter		Nominal Value	Range
Λ_{QCD},	PARJ(81)	0.29	0.28 — 0.31
Q_0,	PARJ(82)	1.0	0.7 — 1.8
σ_q,	PARJ(21)	0.37	0.32 — 0.40
γ_s,	PARJ(2)	0.285	0.250 — 0.320
$[V/(V+S)]_{\mathrm{u,d}}$,	PARJ(11)	0.50	0.30 — 0.75
$[V/(V+S)]_{\mathrm{s}}$,	PARJ(12)	0.60	0.50 — 0.75
$[V/(V+S)]_{\mathrm{c,b}}$,	PARJ(13)	0.75	0.65 — 0.80
ϵ_b,	PARJ(55)	0.0055	0.0025 — 0.0095
ϵ_c,	PARJ(54)	0.05	0.03 — 0.07
direct baryon rate,	PARJ(1)	0.1	0.08 — 0.12
popcorn parameter,	PARJ(5)	1	0 — 2
x_{d},	PARJ(76)	0.7	0 — 0.7
x_{s},	PARJ(77)	∞	0 — ∞

Table 8: The ranges of parameters assumed in the fragmentation and $\mathrm{B^0}$–$\overline{\mathrm{B^0}}$ mixing modelling systematic error study. The corresponding Jetset parameter is also given. These variations are similar to those in [20].

the sample, as the charge bias will differ in the forward and backward hemispheres. The maximum extent of such an effect may be determined using the asymmetry in the rate of γ conversions as a function of $|\cos\theta_{\mathrm{T}}|$. Within the acceptance, this conversion asymmetry is both independent of $\cos\theta$ and consistent with zero to within the 0.7% statistical precision. This uncertainty is combined with the observed charge bias to obtain a relative uncertainty on the final measured $A_{\mathrm{FB}}^{\mathrm{b}}$ of 0.7%.

The determination of the b asymmetry is sensitive to the average tagging efficiencies of the various quark flavours. These have to be known to determine the fraction of the different flavours in the sample. The charm and bottom tagging efficiencies are determined directly from the data, which makes the measurement insensitive to the modelling of the heavy quark fragmentation and decay. The u, d and s tagging efficiencies were determined from Monte Carlo. The efficiency for tagging a b-event, $\overline{\eta_{\mathrm{b}}}$, is found to be 13% higher in the data than the Monte Carlo. This could be due to the incorrect b-lifetimes and mean b-decay multiplicity in the Monte Carlo, or else due to resolution effects in the data that are not modelled in the Monte Carlo. To account for such a possible effect, the tagging efficiencies for the light quarks were increased by 13%, and the resulting change in the measured asymmetry is taken as a systematic uncertainty. Effects due to the fragmentation modelling of u,d and s quarks were found to have a negligible effect on the tagging efficiencies.

The shapes of the quark tagging efficiencies as a function of $|\cos\theta_{\mathrm{T}}|$ are required for the calculation of the acceptance factors C_i. These are taken from the Monte Carlo for the light quarks. In the case of the b-quarks, the efficiency as a function of $|\cos\theta_{\mathrm{T}}|$ was inferred from the single and double tagging rates. The statistical precision of the efficiencies obtained in a similar fashion for the c-quark is poor, and so the b-quark form is assumed. The difference between the factor calculated in this way and that when the Monte Carlo curve was used is small, and included as a systematic error. The shape of the b-quark efficiency curve is parameterised and the change caused by varying the shape according to the fit errors was used to estimate the systematic uncertainty. The various efficiency curves are shown in Fig. 3.

The factors ρ describing the correlation between the tagging efficiencies in the two hemispheres of an event were determined in part from the data and in part from Monte Carlo. For the central value, the non-b events were assumed to have no such correlation. This is supported by the Monte Carlo in the case of the u, d and s quark events. In the case of charm, the correlations were seen to be similar

to those for b-events. However, the effect of the small deviation from unity in the charm case was not seen to change the b- and c-efficiencies determined in the Monte Carlo sample to within the statistical precision for the test. As an estimate of the systematic uncertainty in setting the charm correlation factor to unity, the data efficiencies were re-estimated with the charm correlation factor set equal to that determined for b-events. The change in the resulting b asymmetry was taken as a systematic error. The limited Monte Carlo and data statistics also contribute to the systematic error.

The effects of incorrect modelling of the track resolutions in r-ϕ and $\cos\theta$ in the Monte Carlo on the corrections to the observed quantities were investigated by smearing the Monte Carlo. The factor rescaling the difference between the true and reconstructed values of the r-ϕ track parameters was varied by 20%, while that of the $\cot\theta$ was increased by 100%. As the effect of these resolution changes on the light quark tagging efficiency is smaller than the 13% variation mentioned earlier, it has not been included in this systematic uncertainty to avoid double-counting.

The level to which Jetset Monte Carlo models the mis-estimation of the quark axis by the true thrust axis is not well known. The difference between the asymmetry measured using the true thrust axis and that measured using the quark axis (as determined using correction factors determined with the Jetset Monte Carlo) is therefore taken as a systematic uncertainty in each case.

To investigate any possible sensitivity to the b-tagging cut used, the analysis has been repeated in five bins of increasing L/σ, beginning at $L/\sigma = 4$, each with an approximately equal number of tagged events. The results are statistically consistent with the central value quoted, and no significant trend is observed.

The analysis has also been repeated for different values of κ between 0.3 and 2.0, and after allowing for the correlation between the results at different κ values, no statistically significant differences in the $A_{\rm FB}^{\rm b}$ obtained were observed.

5.3 Monte Carlo Statistics

Monte Carlo events were used to estimate the u, d and s tagging efficiency as well as the properties of the jet charge of $u\overline{u}$, $d\overline{d}$, $s\overline{s}$ and $c\overline{c}$ events. The uncertainties due to Monte Carlo statistics on these parameters are reported in Table 3 and 5.

5.4 Dependence on Standard Model Parameters

The extracted value of $A_{\rm FB}^{\rm b}$ depends on the assumed hadronic partial widths and the forward-backward asymmetries of the non-b events. The partial widths and asymmetries were varied and the gradients, $g(x)$, were calculated for each parameter x, such that:

$$\Delta(A_{\rm FB}^{\rm b}) = g(x)\Delta(x)\,. \tag{18}$$

The gradients obtained are given in Table 9.

The variation with $\Gamma_{b\overline{b}}/\Gamma_{\rm had}$ has the largest gradient, since the selected events are mainly $e^+e^- \to b\overline{b}$. When the assumed value of $\Gamma_{b\overline{b}}/\Gamma_{\rm had}$ is increased the measured asymmetry is reduced. The change in the gradient with centre-of-mass energy reflects the changing relative signs and magnitudes of the asymmetries for b-events and background events. Although the fraction of charm in the sample is larger than u, d or s, the measurement of $A_{\rm FB}^{\rm b}$ is almost completely insensitive to the uncertainty on $\Gamma_{c\overline{c}}/\Gamma_{\rm had}$. This is because the charm partial width enters in the determination of $A_{\rm FB}^{\rm b}$ always as the product $\overline{\eta_{\rm c}} \cdot \frac{\Gamma_{c\overline{c}}}{\Gamma_{\rm had}}$, and therefore a variation of $\Gamma_{c\overline{c}}/\Gamma_{\rm had}$ is compensated by an opposite variation of the charm tagging efficiency $\overline{\eta_{\rm c}}$, which is determined from the data, thus keeping the product about constant. This does not happen in the case of u, d and s, for which the tagging efficiencies are taken from Monte Carlo.

The measured value of $A_{\rm FB}^{\rm b}$ is increased when the assumed value of $A_{\rm FB}^{\rm c}$ is increased. The gradients with respect to the forward-backward asymmetries of u, d and s are small.

	$\sqrt{s}$ = 89.52 GeV	$\sqrt{s}$ = 91.25 GeV	$\sqrt{s}$ = 92.94 GeV
$\Gamma_{b\bar{b}}/\Gamma_{had}$	-0.082	-0.471	-0.855
$\Gamma_{c\bar{c}}/\Gamma_{had}$	< 0.001	$+0.006$	$+0.009$
$\Gamma_{s\bar{s}}/\Gamma_{had}$	-0.002	-0.007	-0.011
$\Gamma_{u\bar{u}}/\Gamma_{had}$	$+0.004$	$+0.015$	$+0.025$
$\Gamma_{d\bar{d}}/\Gamma_{had}$	-0.001	-0.005	-0.009
A^c_{FB}	$+0.065$	$+0.075$	$+0.070$
A^u_{FB}	$+0.020$	$+0.020$	$+0.020$
A^d_{FB}	-0.014	-0.013	-0.014
A^s_{FB}	-0.019	-0.018	-0.018

Table 9: The gradients $g(x)$ of the A^b_{FB} determined below, on and above the peak with respect to the assumed Standard Model parameters, x. The central values assumed are given in Table 4.

5.5 Combined Systematic Uncertainties

The various systematic error sources were combined in quadrature. The asymmetries obtained based on the true thrust axis of all final state particles were therefore:

$$\begin{aligned}
A^b_{FB} &= 0.062 \pm 0.034 \pm 0.002 - 0.082\,\Delta(\Gamma_{b\bar{b}}/\Gamma_{had}) \quad \text{at } \sqrt{s} = 89.52\,\text{GeV},\\
A^b_{FB} &= 0.0963 \pm 0.0067 \pm 0.0038 - 0.471\,\Delta(\Gamma_{b\bar{b}}/\Gamma_{had}) \quad \text{at } \sqrt{s} = 91.25\,\text{GeV},\\
A^b_{FB} &= 0.172 \pm 0.028 \pm 0.007 - 0.855\,\Delta(\Gamma_{b\bar{b}}/\Gamma_{had}) \quad \text{at } \sqrt{s} = 92.94\,\text{GeV},
\end{aligned}$$

where, in each case, the first error is statistical, the second is systematic and the third term gives the variation due to a change $\Delta(\Gamma_{b\bar{b}}/\Gamma_{had})$ in the value of $\Gamma_{b\bar{b}}/\Gamma_{had} = 0.216$ assumed. The dependence on the assumed charm asymmetry at the same energy is $\Delta(A^b_{FB}) \approx +0.07\Delta(A^c_{FB})$. The other Standard Model dependencies are small.

6 The Event-by-Event Method

As an independent check the analysis was performed using a different method, still based on the jet charge determination, which will be referred to as the event-by-event method. In this method the angular distribution of Equation 1 was constructed by estimating event-by-event the direction of the quark emitted in the final state. Within the sample of lifetime tagged events, the jet charge Q_{jet} was computed for each hemisphere using Equation 5 with $\kappa = 0.4$, which optimises the precision of this measurement. In addition only events having hemispheres with jet charges of opposite sign were accepted. The sign of the jet charge was then used to indicate the charge of the primary quark in a given hemisphere. The requirement of oppositely charged hemispheres rejects about 45% of the tagged events, but enhances the probability of correct identification of the direction of the primary quark.

The observed angular distribution of the outgoing quark can be expressed as:

$$\frac{d\sigma^{obs}}{dx} = C(1 + x^2 + \frac{8}{3}A^{obs}_{FB}x)\overline{\eta}(x) \tag{19}$$

where $x = -Q_{jet} \cdot |\cos\theta_T|/|Q_{jet}|$ and Q_{jet} is measured in the forward hemisphere. The constant C is for normalization, and $\overline{\eta}(x)$ is the tagging efficiency as a function of angle for an event. It is assumed that the efficiencies of events for each primary flavour all have the same shape; the systematic error introduced by this assumption is addressed later. It is also assumed that the efficiencies are even functions of x. As a result, the normalisation is independent of A^{obs}_{FB}. The observed asymmetry is defined as:

$$A^{obs}_{FB} = \sum_i s_i F_i (2P_i - 1) A^i_{FB} \tag{20}$$

where s_i is $+1$ for the down-like quarks and -1 for the up-like quarks, and F_i is the fraction of the flavour type i present in the data sample, defined in Equation 16. The term P_i is the probability of correctly identifying the direction of the outgoing quark with flavour i.

Using Equation 19 the observed asymmetry $A_{\rm FB}^{obs}$ was obtained by maximising the log likelihood:

$$\ln \mathcal{L} = \sum_j \ln[C\overline{\eta}(x_j)] + \sum_j \ln[1 + x_j^2 + \frac{8}{3} A_{\rm FB}^{obs} x_j] \tag{21}$$

where the sum is over all the selected events and $A_{\rm FB}^{obs}$ is the only free parameter in the fit. The first term is a constant for a given set of events, so that the efficiency as a function of x, $\overline{\eta}(x_j)$, does not need to be known.

For a given flavour i the fraction of events with opposite jet charges f_{opp}^i, assuming no correlation between hemispheres, is given by:

$$f_{opp}^i = \mathcal{P}_i^2 + (1 - \mathcal{P}_i)^2 \tag{22}$$

where $\mathcal{P}_i$ is the probability of correctly identifying the sign of the charge of the outgoing quark with flavour i in a given hemisphere. The probability P_i of Equation 20 is related to $\mathcal{P}_i$ by the relation:

$$P_i = \mathcal{P}_i^2 / (\mathcal{P}_i^2 + (1 - \mathcal{P}_i)^2)\,. \tag{23}$$

The observed fraction of oppositely charged events in the sample of tagged events, f_{opp}^{obs}, is given by:

$$f_{opp}^{obs} = \sum_i f_{opp}^i \cdot F_i\,. \tag{24}$$

The small correlation between the jet charges of opposite hemispheres was estimated from Monte Carlo, and was taken into account when computing the charge identification probabilities P_i. The values of the probabilities $P_{\rm u}$, $P_{\rm d}$, $P_{\rm s}$ and $P_{\rm c}$ were derived from the Monte Carlo. The charge identification probability for $\rm b\overline{b}$ events was then obtained from the data using Equations 22, 23 and 24. Due to the high b-fraction of the data sample the uncertainties in the modelling of the light flavour fragmentation are expected to have a small effect on the determination of $A_{\rm FB}^{\rm b}$. Table 10 summarises the values of P_i used in the analysis with their statistical errors.

Event Type	Charge id. probability P_i
$\rm b\overline{b}$	0.756 ± 0.005
$\rm c\overline{c}$	0.777 ± 0.001
$\rm u\overline{u}$	0.868 ± 0.001
$\rm d\overline{d}$	0.763 ± 0.001
$\rm s\overline{s}$	0.794 ± 0.001

Table 10: Charge identification probabilities. The values quoted for $\rm b\overline{b}$ were determined from the data, whereas for the other flavours they were obtained from Monte Carlo. The errors are statistical only.

Using the likelihood function given in Equation 21, the data were fitted to obtain the observed asymmetry, which was then corrected to extract $A_{\rm FB}^{\rm b}$ according to Equation 20. The predictions from ZFITTER were used for the u, d, s and c forward-backward asymmetries. For the three different centre-of-mass energy samples, the following asymmetries were obtained:

$$\begin{aligned}
A_{\rm FB}^{\rm b} &= 0.051 \pm 0.038 \pm 0.002 - 0.06\,\Delta(\Gamma_{\rm b\overline{b}}/\Gamma_{\rm had}) \quad \text{at } \sqrt{s} = 89.52\,\text{GeV},\\
A_{\rm FB}^{\rm b} &= 0.1030 \pm 0.0082 \pm 0.0042 - 0.52\,\Delta(\Gamma_{\rm b\overline{b}}/\Gamma_{\rm had}) \quad \text{at } \sqrt{s} = 91.25\,\text{GeV},\\
A_{\rm FB}^{\rm b} &= 0.173 \pm 0.032 \pm 0.009 - 0.94\,\Delta(\Gamma_{\rm b\overline{b}}/\Gamma_{\rm had}) \quad \text{at } \sqrt{s} = 92.94\,\text{GeV},
\end{aligned}$$

where in each case the first error is statistical, the second is systematic and the third term gives the variation due to a change $\Delta(\Gamma_{b\overline{b}}/\Gamma_{had})$ in the value of $\Gamma_{b\overline{b}}/\Gamma_{had} = 0.216$ assumed. The dependence on the assumed charm asymmetry at the same energy is $\Delta(A_{FB}^{b}) \approx +0.09\Delta(A_{FB}^{c})$.

The statistical error includes the statistical uncertainty on the determination of P_b from Equation 23 as well as the statistical uncertainty on the b and c tagging efficiencies from data.

The systematic errors were estimated in the same way as described in Section 5. They are very similar to those in Table 7, though this cross-check method has a larger fragmentation modelling uncertainty. In calculating the b asymmetry using the likelihood fit, it was assumed that the tagging efficiencies for the various quark flavours have the same $|\cos\theta_T|$ dependence. This assumption was tested on both Monte Carlo and data and found to be valid within the statistical uncertainties for $c\overline{c}$ and $b\overline{b}$ which represent almost the entire data sample. The tagging efficiencies for $u\overline{u}$, $d\overline{d}$ and $s\overline{s}$ events seem to have a slightly different shape in the range $0.6 < |\cos\theta_T| < 0.8$. To determine the sensitivity of the measurement to a possible different $|\cos\theta_T|$ dependence of the efficiency for different event types, the $|\cos\theta_T|$ range was divided into two different bins corresponding to $|\cos\theta_T| < 0.6$ and $0.6 < |\cos\theta_T| < 0.8$. In each bin the analysis was repeated independently, using its relative tagging efficiencies, and determining the relative b asymmetry. Then a weighted average of the b asymmetries extracted in this way was computed, which differed by 0.0011 from the asymmetry determined assuming the same efficiency over the whole $|\cos\theta_T|$ range. This difference was included in the systematic error.

The results are in good agreement with the main method. The event sample used is a subset of that used for the main method, and so the results have a high statistical correlation, as well as a significant systematic correlation.

7 Conclusions

The forward-backward asymmetry of the process $e^+e^- \to b\overline{b}$ was measured below, at and above the peak of the Z^0 resonance using a statistical method based on the jet charge. The results are:

$$\begin{aligned}
A_{FB}^{b} &= 0.062 \pm 0.034 \pm 0.002 - 0.082\,\Delta(\Gamma_{b\overline{b}}/\Gamma_{had}) \quad \text{at } \sqrt{s} = 89.52\,\text{GeV},\\
A_{FB}^{b} &= 0.0963 \pm 0.0067 \pm 0.0038 - 0.471\,\Delta(\Gamma_{b\overline{b}}/\Gamma_{had}) \quad \text{at } \sqrt{s} = 91.25\,\text{GeV},\\
A_{FB}^{b} &= 0.172 \pm 0.028 \pm 0.007 - 0.855\,\Delta(\Gamma_{b\overline{b}}/\Gamma_{had}) \quad \text{at } \sqrt{s} = 92.94\,\text{GeV},
\end{aligned}$$

where in each case the first error is statistical, the second is systematic and the third term gives the variation due to a change $\Delta(\Gamma_{b\overline{b}}/\Gamma_{had})$ in the value of $\Gamma_{b\overline{b}}/\Gamma_{had} = 0.216$ assumed. The dependence on the assumed charm asymmetry at the same energy is $\Delta(A_{FB}^{b}) \approx +0.07\Delta(A_{FB}^{c})$. The other Standard Model dependencies are small.

The forward-backward asymmetries of the tagged sample were used to determine the effective weak mixing angle $\sin^2\theta_W^{eff,e}$. In determining the asymmetries quoted above, the values of various quantities that are predicted by the Standard Model had to be assumed, as has been described in subsection 4.2. The analysis was repeated using ZFITTER to predict these Standard Model inputs, with the top mass varied until the χ^2 between the observed and predicted asymmetries on- and off-peak was minimised. The other parameters assumed in ZFITTER were $M_Z = 91.187$ GeV/c^2, $M_{Higgs} = 300$ GeV/c^2, and $\alpha_s = 0.12$. The asymmetries were calculated with correction factors C_i^{quark} appropriate to produce the $\cos\theta_{quark}$ asymmetries. The QCD corrections to the A_{FB}^{b} values were *not* applied, being largely inherent in the method. The $\sin^2\theta_W^{eff,e}$ of the electron channel which corresponded to the top quark mass, M_{top}, that minimised the χ^2 was evaluated, where $\sin^2\theta_W^{eff,e}$ is defined by Equation 4. The measured asymmetries along with the Standard Model prediction (using the fitted value of $\sin^2\theta_W^{eff,e}$) are shown in Fig. 4. The result for $\sin^2\theta_W^{eff,e}$ is:

$$\sin^2\theta_W^{eff,e} = 0.2313 \pm 0.0012 \pm 0.0006$$

which corresponds to $M_{\rm top} = 196^{+33\ +16}_{-38\ -19}\,{\rm GeV}/c^2$, where the first error is statistical and the second is systematic. A variation in the assumed mass of the Higgs boson between 60 and 1000 GeV/c^2 corresponds to an uncertainty in $\sin^2\theta_{\rm W}^{\rm eff,e}$ of ± 0.00006 and on $M_{\rm top}$ of $^{+20}_{-26}$ GeV/c^2. This indirect determination of the top quark mass is in good agreement with those from direct observation [22,23]. The $\sin^2\theta_{\rm W}^{\rm eff,e}$ agrees with that determined in a similar recent analysis using jet charges [4], with the most precise currently published determination of $A_{\rm FB}^{\rm b}$ from fits to inclusive lepton spectra [24] and with that determined from a recent measurement of $A_{\rm FB}^{\rm b}$ and $A_{\rm FB}^{\rm c}$ using a combination of inclusive lepton and jet charge information [5]; these results are compared in Table 11.

	Method	$\sin^2\theta_{\rm W}^{\rm eff,e}$
This analysis	jet charges	0.2313 ± 0.0013
ALEPH [4]	jet charges	0.2315 ± 0.0018
L3 [24]	leptons	0.2335 ± 0.0021
DELPHI [5]	leptons and jet charges	0.2294 ± 0.0021

Table 11: A comparison of various recent determinations of $\sin^2\theta_{\rm W}^{\rm eff,e}$ associated with $A_{\rm FB}^{\rm b}$ measurements by the LEP experiments.

A Relating $\langle \mathbf{Q_F} \cdot \mathbf{Q_B} \rangle$ to the Charge Separation δ

We define Q_F and Q_B as the jet charges measured in the forward and backward hemispheres. Using these jet charges we measure the quantities $\langle Q_F - Q_B \rangle$ and $\langle Q_F \cdot Q_B \rangle$. We also measure the mean, $\mu(Q)$, and width, $\sigma(Q)$, of the distribution of jet charge for all forward and backward hemispheres. These distributions have exactly equal contributions from positive and negative quarks. In the Monte Carlo it is also possible to decide which of these charges corresponds to the jet charge of the negatively charged quark and which corresponds to the positively charged quark. These we define as Q_- and Q_+ respectively.

Starting from the definition of the covariance of Q_- and Q_+,

$$\begin{aligned} \mathrm{cov}[Q_-, Q_+] &= \langle Q_- Q_+ \rangle - \langle Q_- \rangle \langle Q_+ \rangle \\ &= \langle Q_- Q_+ \rangle + \frac{1}{4}(\delta^2 - \xi^2) \end{aligned} \tag{25}$$

where

$$\begin{aligned} \delta &= \langle Q_- \rangle - \langle Q_+ \rangle \\ \xi &= \langle Q_- \rangle + \langle Q_+ \rangle = 2\mu(Q). \end{aligned}$$

The quantity δ is called the *charge separation* and ξ is termed the *charge offset*. If the jet charge is an estimator of the quark charge then δ will have some non-zero value. If the detector has a different response to positively and negatively charged quarks then ξ will also have some non-zero value. Using $\langle Q_F Q_B \rangle = \langle Q_- Q_+ \rangle$ and $\xi^2 = 4\mu^2(Q)$ and rearranging Equation 25 gives:

$$\begin{aligned} \delta^2 &= 4\{-\langle Q_- Q_+ \rangle + \mathrm{cov}[Q_-, Q_+]\} + \xi^2 \\ &= 4\{-\langle Q_F Q_B \rangle + \mathrm{cov}[Q_-, Q_+] + \mu^2(Q)\}. \end{aligned} \tag{26}$$

This is the important result; it will now be refined to write it explicitly referring to a correlation coefficient.

If we assume that $\sigma(Q_-) = \sigma(Q_+)$, confirmed by the Monte Carlo, then the covariance term of Equation 26 can be rewritten in the following way:

$$\begin{aligned} \mathrm{cov}[Q_-, Q_+] &= \rho[Q_-, Q_+]\sigma(Q_-)\,\sigma(Q_+) \\ &= \rho[Q_-, Q_+](\sigma^2(Q) - \frac{1}{4}\delta^2) \end{aligned}$$

where we have used:

$$\begin{aligned} \sigma^2(Q) &= \langle Q^2 \rangle - \langle Q \rangle^2 \\ &= \frac{1}{2}\langle Q_-^2 \rangle + \frac{1}{2}\langle Q_+^2 \rangle - (\frac{1}{2}\langle Q_- \rangle + \frac{1}{2}\langle Q_+ \rangle)^2 \\ &= \frac{1}{2}\sigma^2(Q_-) + \frac{1}{2}\sigma^2(Q_+) + \frac{1}{4}\delta^2. \end{aligned} \tag{27}$$

The expression for δ then becomes:

$$\delta^2 = 4\left(\frac{-\langle Q_F Q_B \rangle + \rho[Q_-, Q_+]\sigma^2(Q) + \mu^2(Q)}{1 + \rho[Q_-, Q_+]}\right),$$

which is the form used in the analysis.

Acknowledgements:

It is a pleasure to thank the SL Division for the efficient operation of the LEP accelerator, the precise information on the absolute energy, and their continuing close cooperation with our experimental group. In addition to the support staff at our own institutions we are pleased to acknowledge the
Department of Energy, USA,
National Science Foundation, USA,
Particle Physics and Astronomy Research Council, UK,
Natural Sciences and Engineering Research Council, Canada,
Fussefeld Foundation,
Israel Ministry of Science,
Israel Science Foundation, administered by the Israel Academy of Science and Humanities,
Minerva Gesellschaft,
Japanese Ministry of Education, Science and Culture (the Monbusho) and a grant under the Monbusho International Science Research Program,
German Israeli Bi-national Science Foundation (GIF),
Direction des Sciences de la Matière du Commissariat à l'Energie Atomique, France,
Bundesministerium für Forschung und Technologie, Germany,
National Research Council of Canada,
A.P. Sloan Foundation and Junta Nacional de Investigaccão Científica e Tecnológica, Portugal.

References

[1] *Z Physics at LEP 1 - Volume 1*, Edited by G. Altarelli, CERN 89-08, September 1989.

[2] OPAL Collaboration, P. Acton *et al.*, Z. Phys. **C60** (1993) 19.

[3] T. Behnke and D. G. Charlton, *Electroweak Measurements using Heavy Quarks at LEP*, CERN-PPE/95-11, January 1995, submitted to Physica Scripta.

[4] ALEPH Collaboration, D. Decamp *et al.*, Phys. Lett. **B335** (1994) 99.

[5] DELPHI Collaboration, P. Abreu *et al.*, Z. Phys. **C65** (1995) 569.

[6] OPAL Collaboration, K. Ahmet *et al.*, Nucl. Instrum. Methods **A305** (1991) 275;
P. P. Allport *et al.*, Nucl. Inst. and Meth. **A324** (1993) 34;
P. P. Allport *et al.*, Nucl. Inst. and Meth. **A346** (1994) 479.

[7] OPAL Collaboration, G. Alexander *et al.*, Z. Phys. **C52** (1991) 175.

[8] JADE Collaboration, W. Bartel *et al.*, Z. Phys. **C33** (1986) 23;
JADE Collaboration, S. Bethke *et al.*, Phys. Lett. **B213** (1988) 235.

[9] OPAL Collaboration, M. Z. Akrawy *et al.*, Z. Phys. **C49** (1991) 375.

[10] T. Sjöstrand, Comp. Phys. Comm. **39** (1986) 347;
T. Sjöstrand and M. Bengtsson, Comp. Phys. Comm. **43** (1987) 367;
T. Sjöstrand, CERN-TH.6488/92. OPAL optimised parameters were used, as described in
OPAL Collaboration, M. Z. Akrawy *et al.*, Z. Phys. **C47** (1990) 505 and
OPAL Collaboration, P. Acton *et al.*, Z. Phys. **C58** (1993) 387.

[11] J. Allison *et al.,* Phys. Rev. **A317** (1992) 47.

[12] G. Marchesini *et al.*, Comp. Phys. Comm. **67** (1992) 465.

[13] C. Peterson, D.Schlatter, I.Schmitt and P.M.Zerwas, Phys. Rev. **D27** (1983) 105.

[14] ALEPH Collaboration, D. Decamp *et al.*, Phys. Lett. **B244** (1990) 551;
ALEPH Collaboration, D. Decamp *et al.*, Phys. Lett. **B266** (1991) 218;
DELPHI Collaboration, P. Abreu *et al.*, Z. Phys. **C56** (1992) 47;
L3 Collaboration, B. Adeva *et al.*, Phys. Lett. **B261** (1991) 177;
OPAL Collaboration, G. Alexander *et al.*, Phys. Lett. **B262** (1991) 341;
OPAL Collaboration, M. Z. Akrawy *et al.*, Phys. Lett. **B263** (1991) 311;
OPAL Collaboration, R. Akers *et al.*, Z. Phys. **C60** (1993) 199;
OPAL Collaboration, R. Akers *et al.*, Z. Phys. **C60** (1993) 601.

[15] OPAL Collaboration, R. Akers *et al.*, Z. Phys. **C65** (1995) 17.

[16] R. D. Field and R. P. Feynman, Nucl. Phys. **B136** (1978) 1.

[17] D. Bardin *et al.*, CERN-TH 6443/92, May 1992.

[18] *Review of Particle Properties*, Particle Data Group, Phys. Rev. **D50** (1994) 1173.

[19] R. Barlow, J. Comp. Phys. **72** (1987) 202.

[20] OPAL Collaboration, P. Acton *et al.*, Phys. Lett. **B294** (1992) 436.

[21] OPAL Collaboration, R. Akers *et al.*, Z. Phys. **C61** (1994) 209.

[22] The CDF Collaboration, F. Abe *et al.*, FERMILAB-PUB-95/022-E, February 1995, submitted to Phys. Rev. Lett.

[23] The D0 Collaboration, S. Abachi *et al.*, FERMILAB-PUB-95/028-E, February 1995, submitted to Phys. Rev. Let.

[24] The L3 Collaboration, M. Acciarri *et al.*, Phys. Lett. **B335** (1994) 542.

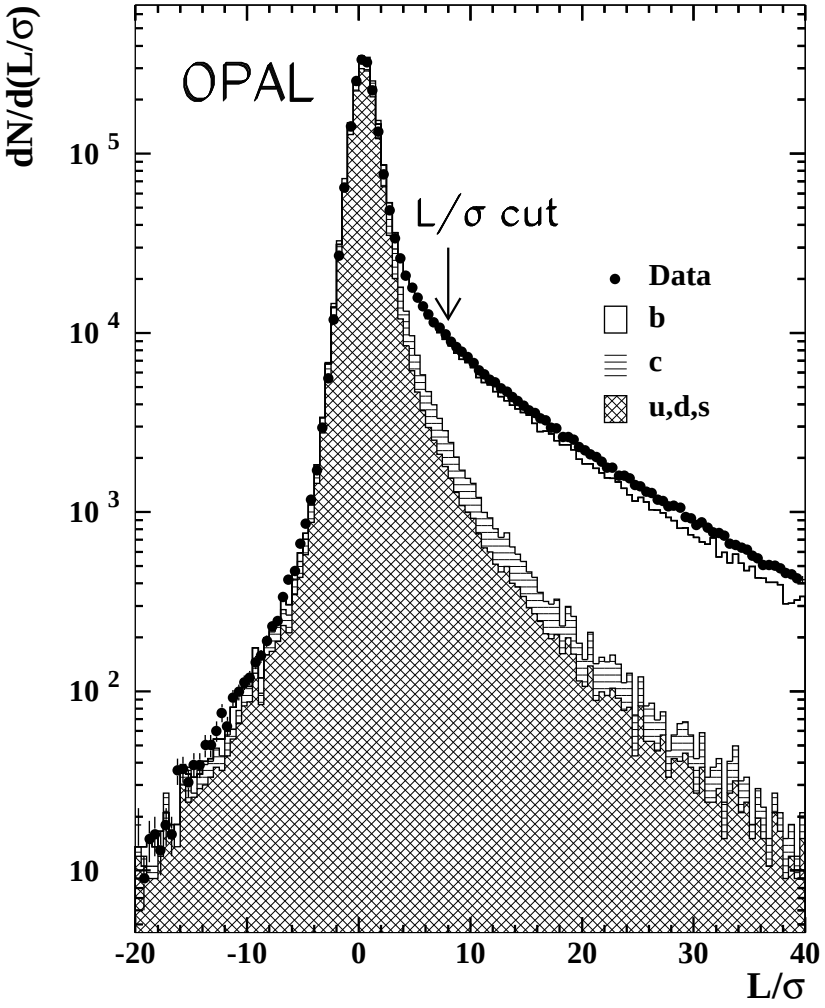

Figure 1: Decay length significance distribution of the most significant secondary vertex in an event. The dots represent the data, superimposed on the Monte Carlo. Both distributions are normalised to the same number of events. The charm and light flavour expected contributions are shown. The L/σ cut is also shown. The Monte Carlo and data disagree for large positive L/σ. This is not relevant for the analysis, since the b tagging efficiency is determined from the data.

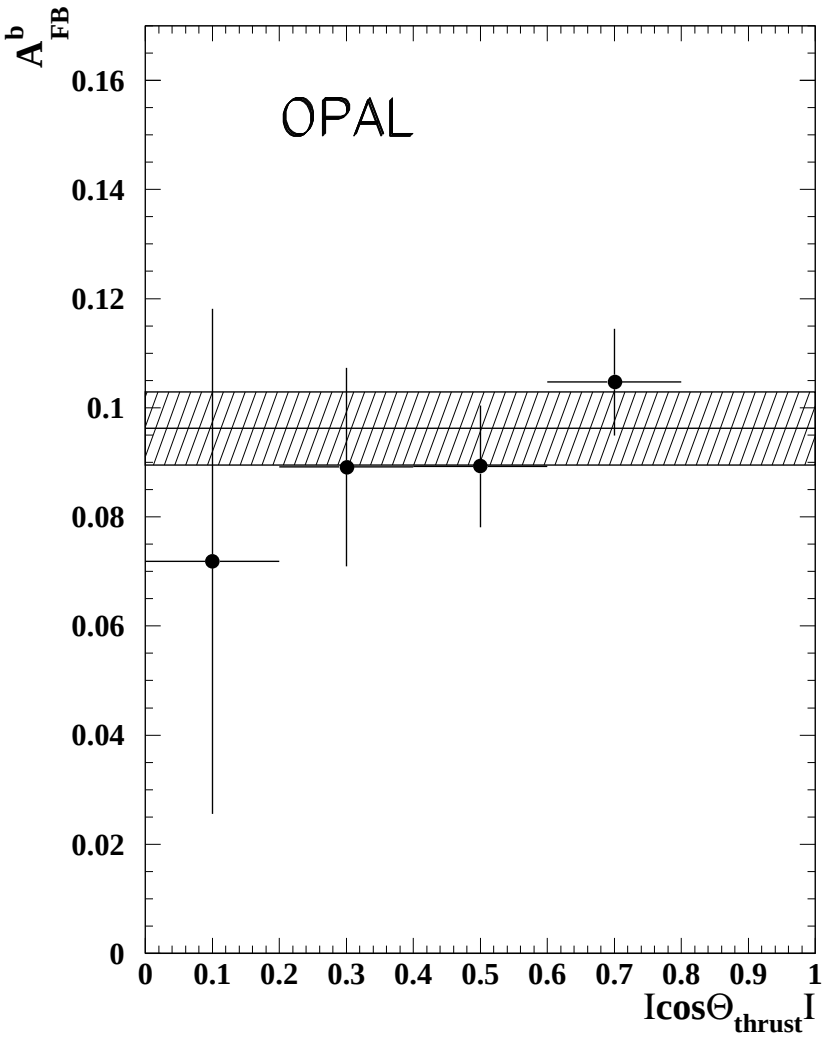

Figure 2: $A_{\rm FB}^{\rm b}$ in bins of $|\cos\theta_{\rm T}|$. The line and shaded area indicate the weighted average of the results and its error. All errors are statistical only.

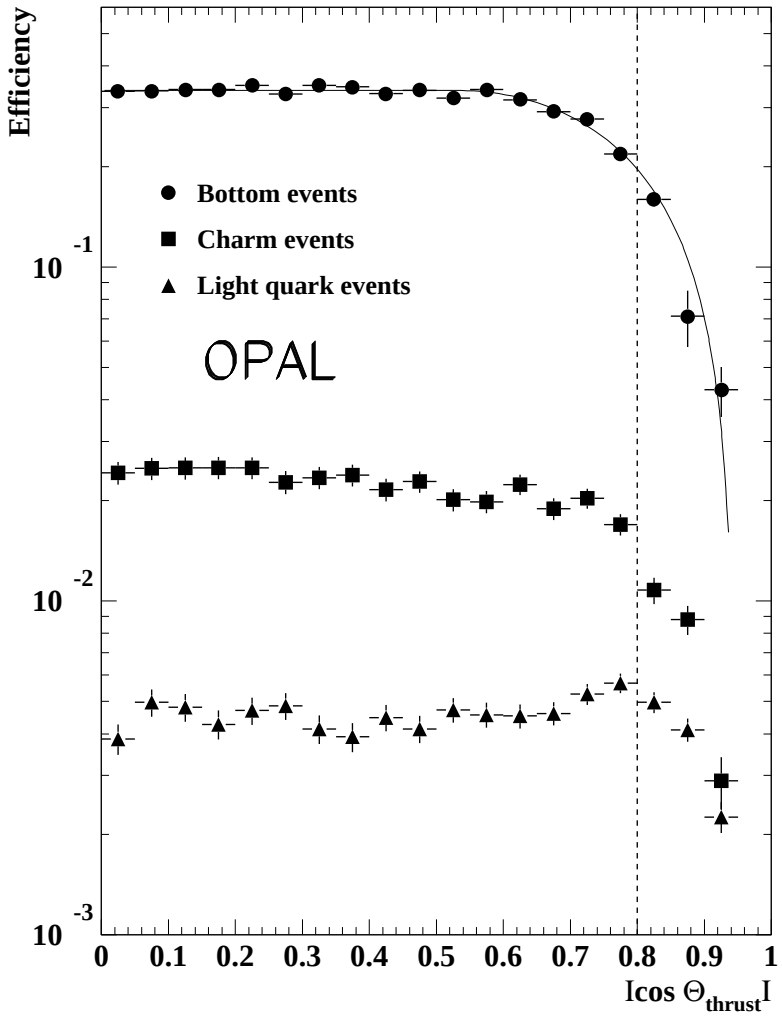

Figure 3: The tagging efficiency for bottom, charm and light quark events as a function of $|\cos\theta_{\mathrm{T}}|$. The b-quark values are taken from the data, the charm and light quark values are taken from the Monte Carlo. The curve is a parameterisation of the points in the region $|\cos\theta_{\mathrm{T}}| < 0.8$.

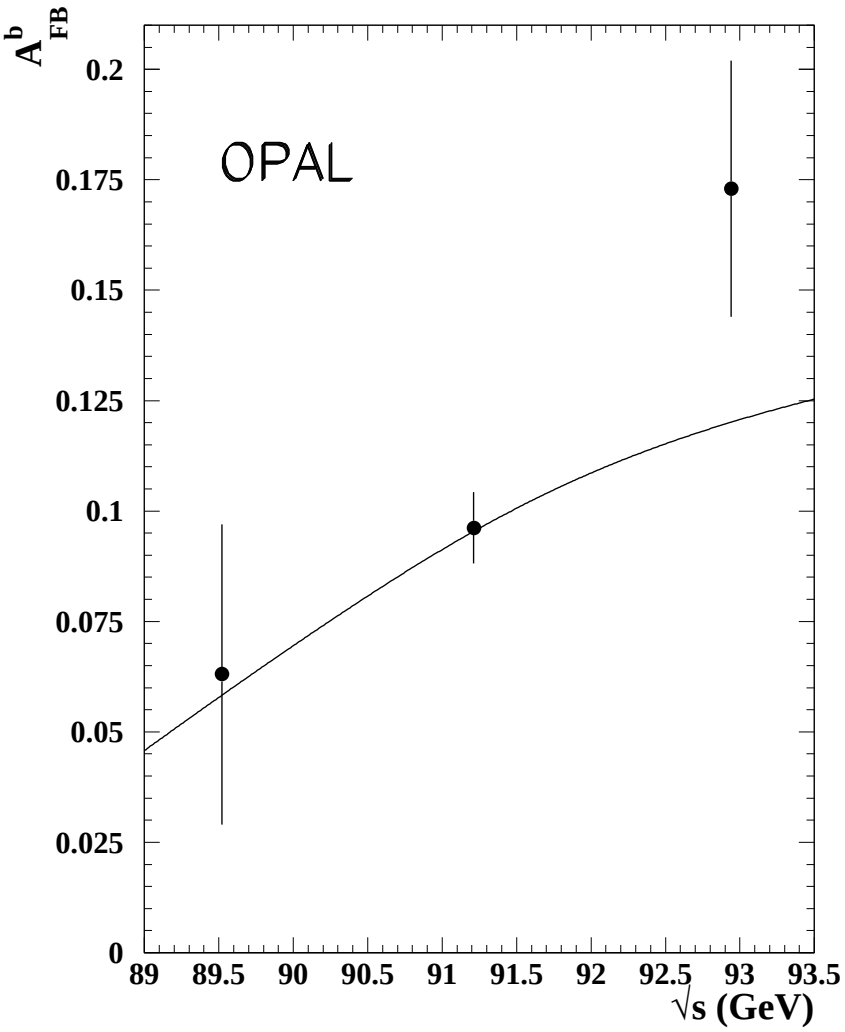

Figure 4: The measured values of $A^{\mathrm{b}}_{\mathrm{FB}}$ as a function of the centre of mass energy. The curve is the Standard Model prediction for $A^{\mathrm{b}}_{\mathrm{FB}}$ using the fitted value of $\sin^2\theta^{\mathrm{eff,e}}_{\mathrm{W}}$.